The 6th International Supercritical CO_2 Power Cycles Symposium
March 27 - 29, 2018, Pittsburgh, Pennsylvania

Oxy-Combustion Flame Fundamentals for Supercritical CO_2 Power Cycles

Peter A. Strakey
Research Scientist
National Energy Technology Laboratory
Morgantown, WV 26507
peter.strakey@netl.doe.gov

Dr. Strakey is a research scientist at the National Energy Technology Laboratory in Morgantown, WV. He received his PhD in mechanical engineering from the Pennsylvania State University and spent the next 10 years studying rocket injector sprays and high-pressure combustion at the Air Force Research Laboratory at Edwards Air Force Base in California. During this time he gained expertise in high-pressure experimentation and laser diagnostics as well as Computational Fluid Dynamics. In 2004 he moved back to the east coast to work in the fossil energy power generation field at NETL. Since then he has focused his research in gas turbine combustion, pressure gain combustion and model validation.

Abstract

Supercritical CO_2 power cycles for fossil energy power generation will likely employ oxy-combustion at very high pressures, possibly exceeding 300 bar. At these high pressures, a direct fired oxy-combustor is more likely to behave like a rocket engine than any type of conventional gas turbine combustor. Issues such as injector design, wall heat transfer and combustion dynamics may play a challenging role in combustor design. Computational Fluid Dynamics (CFD) modeling will not only be useful, but may be a necessity in the combustor design process. To accurately model turbulent reacting flows, combustion sub-models appropriate for the conditions of interest as defined by the turbulent time and length scales as well as chemical kinetic time scales are necessary. The first step in identifying an appropriate modeling approach is to identify what those scales are. As the pressures and energy release densities are much higher than conventional gas turbine or internal combustion engines, it is expected that the time and length scales may be very different and may necessitate alternative modeling approaches.

This paper attempts to estimate approximate turbulent time and length scales as well as chemical kinetic time scales such as turbulent flame speed and ignition delay time at the conditions of interest with the aid of CFD as well as simplified 0-D and 1-D flame calculations. Detailed and reduced chemical kinetic mechanisms for the oxidation of methane at high pressure are also discussed. Finally, a series of CFD Large

Eddy Simulations is presented to investigate the effect of oxygen concentration and carbon dioxide flow-split on combustion behavior.

Introduction

The vast majority of experience within the combustion community in designing and operating gas turbine combustors is at pressures below about 30 bar. Even the highest-pressure aviation gas turbine engines operate below 50 bar [1]. Very little data exists for combustors operating at or near the conditions of the Allam cycle which is currently the forerunner for direct fired sCO_2 power cycles. The closest combustor relatives are liquid rocket engine combustors which can operate at pressures in excess of 370 bar (SSME pre-burner)[2]. Unfortunately, there is very little experimental data from the rocket community detailed enough to validate combustion models. Most rocket engine tests quantify macroscopic parameters such as pressure, thrust, heat load, lifetime, etc. Also, rocket engine combustors usually operate very close to stoichiometric and do not employ exhaust gas dilution as would likely be found in a direct fired sCO_2 combustor which would likely employ some quantity of CO_2 as a diluent to moderate combustor exit temperature.

The Allam cycle [3-4] is a heavily recuperated sCO_2 cycle with only a modest temperature rise in the combustor. The nominal conditions as defined by the Allam cycle include a combustor operating pressure of 300 bar, an inlet temperature of 750 °C and an exit temperature of 1150 °C. The fuel could be either natural gas or syngas derived from a coal gasification process. Published data on the potential thermodynamic efficiency of the cycle are in excess of 58% (for the natural gas version) based on the Lower Heating Value (LHV) of the fuel. Another attractive feature of the cycle is the amenability to carbon capture since the working fluid is nearly pure CO_2 at 300 bar after water removal and compression. In order to maintain a combustor exit temperature of 1150 °C roughly 95% of the CO_2 must be recycled to the combustor with the remainder either vented or sequestered.

With natural gas as the fuel, a stoichiometric amount of O_2 would be roughly 7% of the CO_2 flow by volume. Note that since the oxygen is being produced by an Air Separation Unit (ASU) for this cycle, the O_2 and CO_2 being injected into the head end of the combustor can be mixed in any ratio desired with the balance of the CO_2 being added further downstream. The lower bound of O_2 concentration would be 7% by volume assuming all of the recycled CO_2 is mixed in with the oxygen. An upper bound for O_2 concentration can be set at about 30% by volume based on oxygen safety issues in the piping and recuperators.

With these bounds set on the operating conditions of the combustor it is easy to see why oxy-combustion for direct fired cycles is so unique. High pressure, high preheat temperature and large amounts of CO_2 dilution make this environment significantly different from conventional air breathing gas turbines.

Pressure Effects on Chemistry

Laminar premixed flame speed is a combustion parameter in the form of velocity that is often used to characterize reactant consumption or reaction rates, even in turbulent environments. For premixed

laminar flames, the flame speed S_L is proportional to the reaction rate and molecular diffusivity through the relation:

$$S_L \propto \sqrt{RR \cdot D} \qquad \text{Eqn. 1}$$

Since molecular diffusivity, D, is proportional to 1/P, for a second order reaction, the reaction rate would be proportional to P^2 and S_L would be proportional to $P^{1/2}$. Figure 1 is a plot of premixed laminar flame speed calculated with Cantera [5] using the GRI 3.0 [6] methane oxidation mechanism for CH_4/air as well as $CH_4/O_2/CO_2$ at the same adiabatic flame temperature. Since the flame speed is observed to decrease with increasing pressure it can be deduced that the overall reaction order is about 1.4 for the $CH_4/O_2/CO_2$ case.

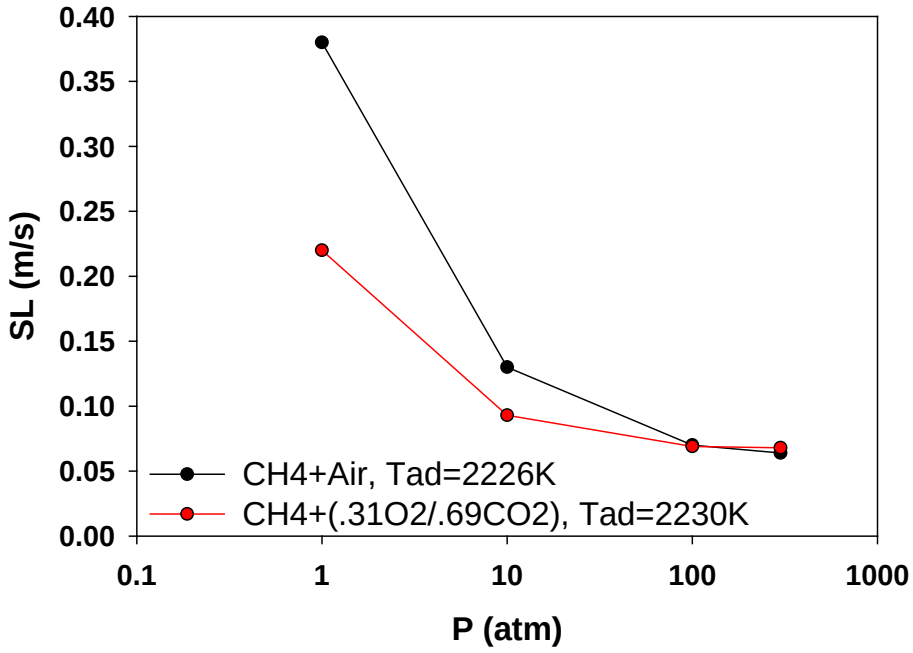

Figure 1: Calculated laminar flame speed for methane/air and methane/O_2/CO_2 as a function of pressure at similar adiabatic flame temperatures.

The laminar flame thickness is given by:

$$\delta_L = \frac{\alpha}{S_L} \qquad \text{Eqn. 2}$$

Where the thermal diffusivity, $\alpha = {}^{k}/_{\rho C_P}$. Since thermal conductivity, k and specific heat, C_P are mostly insensitive to pressure and ρ is proportional to pressure for an ideal gas, the thermal diffusivity is inversely proportional to pressure and the laminar flame thickness is found to also found to decrease with pressure. The net result is that high pressure flames are thinner and propagate more slowly than low pressure flames.

Flame thinning can most easily be seen in an opposed flow flame calculation as shown in Figure 2. This simulation was performed for an opposed flow of methane on one side and an oxidizer consisting of 31% O_2 and 69% CO_2 by volume on the other side. The separation distance was 2 cm and the inlet velocity on both sides was 27 cm/s resulting in a relatively low peak strain rate of about 50 s^{-1} in the flame. The inlet temperature for both fuel and oxidizer was 300 K with the fuel entering on the left side (axial position of 0 cm). The thinning of the reaction zone as pressure increases is evident both in the temperature profiles as well as the OH mole fraction profiles. The shift in the peak temperature and OH mole fraction is due to a slight shift in the stagnation zone as pressure increased. Also note the decrease in peak OH mole fraction as pressure was increased, even though peak temperature actually increased with pressure. This is due to three body recombination reactions depleting the radical pool as pressure is increased.

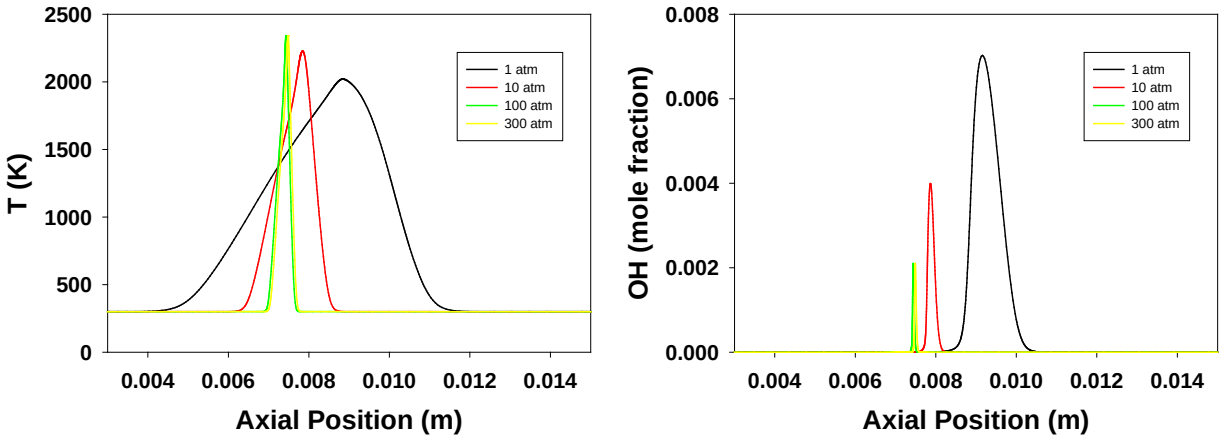

Figure 2: Non-premixed opposed flow flame calculations for methane and O_2+CO_2 as a function of pressure. Temperature profiles (a) and OH mole fraction profiles (b).

Autoignition delay time is also an important chemical time scale in combustion. Depending on the concentration of oxygen delivered to the reaction zone of the combustor, the Damkohler number ($Da=\tau_{turb}/\tau_{chem}$) may be small and the heat release may be more of a stirred reactor where the reactions may be governed more by ignition delay than flame speed. Ignition delay generally decreases with increasing pressure or preheat temperature as seen in Figure 3(a) which shows a comparison of ignition delay times for stoichiometric oxy-combustion of methane with two different oxygen concentrations that span the range of anticipated levels for the Allam cycle. At a pressure of 300 bar, the ignition delay ranges from about 1 to 3 msec. These calculations were performed with the Saudi Aramco 2.0 [7] mechanism which has been validated at pressure much higher than GRI 3.0 [8-9].

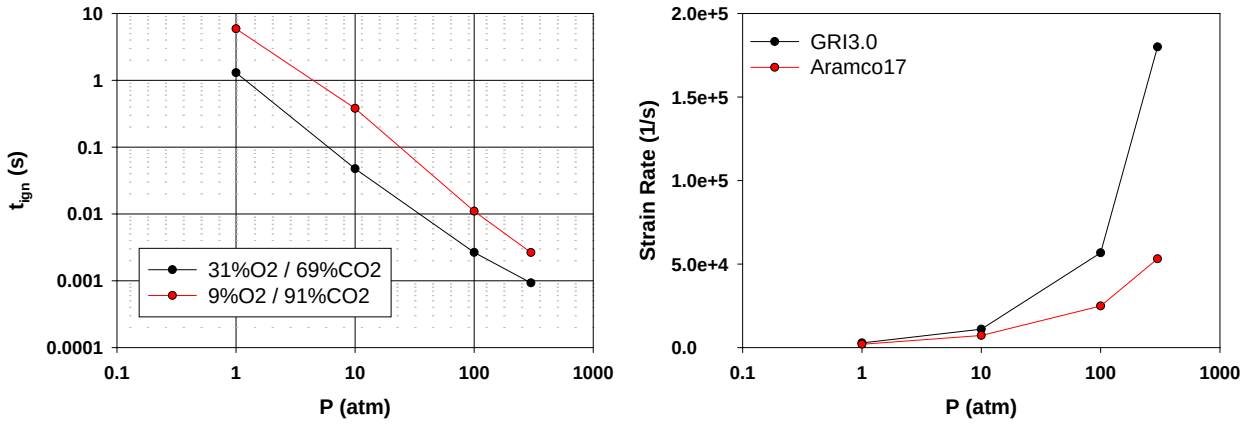

Figure 3: (a) Calculated ignition delay time for two methane/O_2/CO_2 mixtures. (b) Calculated extinction strain rate for a non-premixed flame of methane and 31%O_2/69%CO_2 at 300 bar and 985 K.

Finally, extinction strain rate for a non-premixed counter-flow flame is presented in Figure 3(b) for both the GRI 3.0 and Saudi Aramco mechanisms at a pressure of 300 bar and preheat temperature of 985K. The extinction strain rate is the maximum strain a laminar flame may sustain without extinguishing. Figure 3(b) shows that the extinction strain rate increases with increasing pressure, mainly due to the thinning of the reaction zone as pressure increases. The implication of this is that even as laminar propagation velocity decreases with increasing pressure, the flame will withstand much higher levels of turbulence without quenching. Note the significant discrepancy between the two chemical mechanisms.

Turbulent Time and Length Scales

The usual method of describing the expected regime of combustion for a given system is to use the Borghi diagram [10] (Figure 4) which shows the spectrum of turbulent combustion ranging from laminar flamelets to the stirred reactor regime as a function of non-dimensional velocity and length scales. The velocity scale is the turbulent fluctuating velocity, u' normalized by the laminar flame speed (u'/S_L). The non-dimensional length scale is the integral turbulent length scale normalized by the laminar flame thickness (l_T/δ_L). Figure 4 also shows the typical operating regimes of gas turbines and internal combustion engines.

In an effort to estimate the expected combustion regime for direct-fired sCO_2 combustors, which is important for selecting an appropriate turbulent combustion model [11], the turbulent time and length scales need to be estimated and these are highly geometry dependent. The approach used here is to design and model, using CFD, a canonical combustor scaled to a 50 MW operating condition, which is a reasonable size for a pilot-scale power plant. Since the operating pressure is more in line with rocket engines than gas turbines, the Space Shuttle Main Engine (SSME) pre-burner [2] was used as a model and scaled to Allam cycle conditions. Figure 5 shows the conceptual combustor which contains 21 coaxial type injectors with the oxidizer (O_2+CO_2) flowing on the outside of the fuel (CH_4) stream. The remaining CO_2 is injected through a slot along the wall to provide wall cooling. The combustor includes a transition

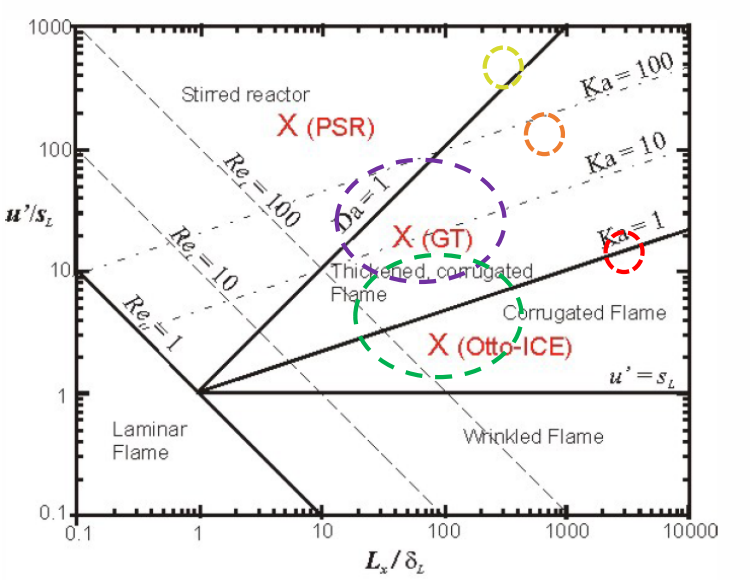

Figure 4: Borghi combustion diagram with estimated operating conditions for direct-fired oxy-combustion at three levels of oxygen concentration. Conventional gas turbines and IC engine regimes shown for reference.

section on the aft end to accelerate the combustion gases towards a turbine inlet. The combustor exit was assumed to be a constant pressure boundary for the cases presented here. The combustor was meshed with a combination of polyhedral and hexahedral cells with a total cell count of 3.9 million cells.

Simulations were conducted using the commercial CFD code ANSYS Fluent 16.2 [12] with a Reynolds Averaged Navier-Stokes (RANS) turbulence modeling approach. A simple, two equation k-epsilon turbulence model was used with a 19-species skeletal methane oxidation mechanism and no turbulence

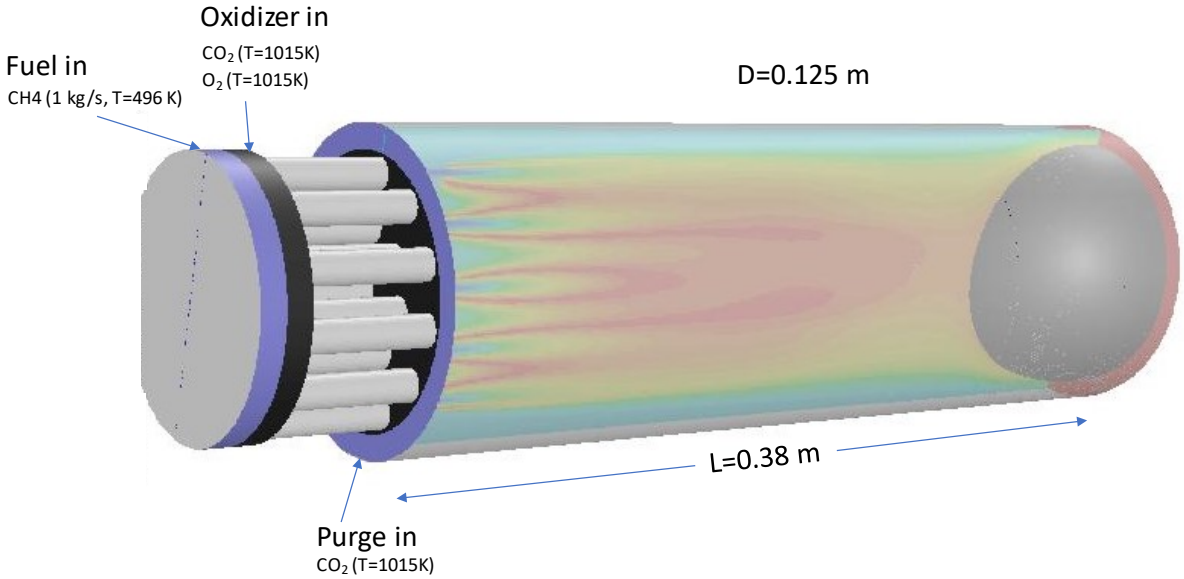

Figure 5: Conceptual oxy-combustor for CFD modeling using 21 coaxial injectors.

chemistry interaction model. The integral length scale is derived from the calculated turbulence field according to:

$$l_T = 0.37\frac{u'^3}{\varepsilon} = 0.20\frac{k^{1/2}}{\varepsilon} \qquad \text{Eqn. 3}$$

where u' is calculated from:

$$u' = \sqrt{\frac{2k}{3}} \qquad \text{Eqn. 4}$$

The methane flowrate for all three cases was 1 kg/s representing an equivalence ratio of 0.95. The three simulations span a range of oxygen concentration in the injectors from 9% to 31% by volume with the balance being CO_2. Table 1 contains a comparison of time and length scales computed from the CFD simulations along with the laminar flame speed and ignition delay time calculated from Cantera. While the integral length scale for all three simulations was very similar (~2 mm), the turbulent fluctuating velocity for the 9% oxygen case was much higher than the 31% oxygen case. This was due to the fact that having all of the CO_2 passing through the injectors for the 9% O_2 case resulted in a significantly higher bulk flow velocity in the reaction zone (70 m/s vs. 30 m/s). Figure 6 shows a comparison of temperature contours for the highest and lowest oxygen concentration (case 1 and case 3) from the RANS simulations at 300 bar.

Table 1: Operating conditions and resulting length, time and velocity scales for the three cases studied.

parameter	Case 1	Case 2	Case 3
O_2 mole fraction	0.31	0.18	0.09
U_{bulk} (m/s)	30	35	70
l_T (m)	1.9e-3	2.2e-3	2.0e-3
U' (m/s)	7.5	10.7	23.8
S_L (m/s)	0.58	0.082	0.05
τ_{ign} (s)	9.2e-4	1.6e-3	2.5e-3

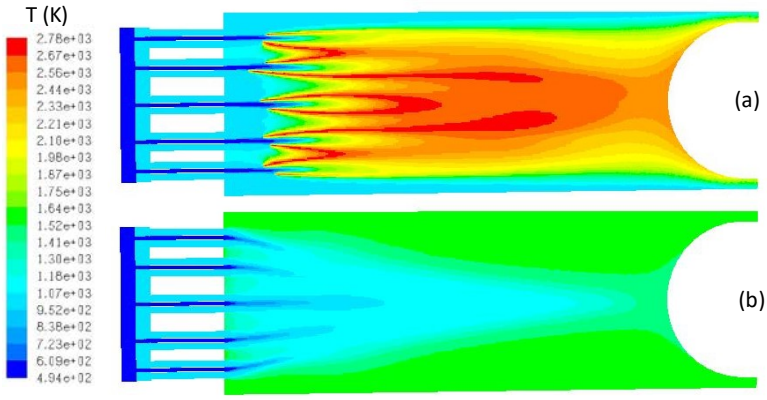

Figure 6: Temperature contours from RANS simulations for case 1 (a), and case 3 (b).

When plotted on the Borghi combustion diagram (Figure 4) the oxy combustion cases span the range of combustion regime from corrugated flamelets to stirred reactor. On implication of this is that an appropriate turbulence chemistry interaction model for high fidelity CFD simulations may vary depending on the conditions, in this case oxygen concentration. A flamelet model, which would likely perform well for the 31% O_2 case may perform poorly for the 9% O_2 case which is governed more by autoignition than flame propagation. Also of note in Figure 4 is the placement on the diagram in relation to the gas turbine and IC engine range of conditions. For high pressure oxy-combustion, the Reynolds number and/or Karlovitz number ($Ka=\tau_{chem}/\tau_K$) are significantly larger than gas turbines or IC engines which may render some of the conventional turbulence chemistry interaction models less valid. At the very least, these results indicate the need for validation data at high-pressure oxy-combustion conditions.

Chemical Kinetic Mechanisms

Accurate modeling of combustion processes requires a chemical kinetic mechanism valid for the range of conditions being studied. Unfortunately, for high-pressure oxy-combustion, there are no validated mechanisms available. The most commonly used mechanism for methane oxidation, GRI 3.0 [6], has only been validated at pressures up to about 30 bar with most of the target validation data being for pressures less than 10 bar. A more recently developed mechanism, referred to as Saudi Aramco 2.0 mechanism, developed by the National University of Ireland Galway [7] has been validated against laminar flame speed data at pressure up to 60 bar [8] with methane, oxygen and helium and ignition delay time data up to 260 bar [9] with methane, oxygen and argon mixtures. While lacking validation data with CO_2 dilution and pressures up to Allam cycle conditions, this is one of the closest relevant mechanisms. This very large mechanism, even after being pared down to include just C_2 and smaller hydrocarbons includes 103 species and 480 reactions. While this is not an issue for 0D and 1D calculations, a mechanism of this size needs to be further reduced into a skeletal mechanism in order to be useful for CFD simulations.

The simplest way to achieve this is through sensitivity analysis using a combination of laminar flame speed and with stirred reactor calculations to determine the most important species and reactions. This analysis was performed using stoichiometric methane/oxygen/carbon dioxide mixtures at pressures and temperatures relevant to the Allam cycle to generate several skeletal mechanisms with a target of 15 to

35 species. The skeletal mechanisms were then used to predict laminar flame speed for methane/oxygen/helium mixtures at 60 bar, where experimental data is available. The results are presented in Figure 7(a) along with the experimental data of Rozenchan et al [8] as well as predictions with both the parent Saudi Aramco 2.0 mechanism as well as GRI 3.0. For these conditions it is evident that the Saudi Armco mechanism, while overpredicting the laminar flame speed, is closer to the experimental data than GRI 3.0. The performance of the various skeletal mechanism generally improves in agreement with the parent mechanism with an increase in the number of species in the mechanism.

A comparison of calculated ignition delay time as a function of pressure is shown in Figure 7(b) for a stoichiometric methane/oxygen/carbon dioxide mixture with an initial temperature of 985 K and an initial oxygen molar concentration of 27%. Figure 7 Illustrates the general improvement in agreement between the skeletal mechanisms and the parent mechanism as the number of included species is increased. Figure 7(b) also shows a significant variation in ignition delay time at 300 bar between the two detailed mechanisms, GRI 3.0 and Saudi Aramco 2.0. Clearly, more experimental data is needed at very high pressures in order to validate or refine the detailed mechanisms.

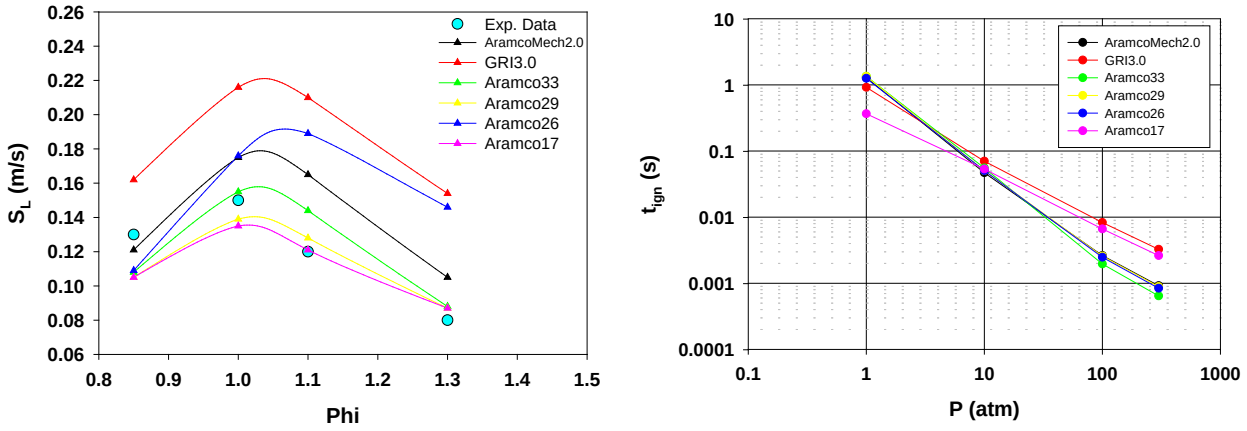

Figure 7: Calculated laminar flame speeds (a) vs phi for a CH_4+(.15O_2/.85HE) blend at 60 bar and 298 K, and ignition delay time (b) vs pressure for a stoichiometric (.13CH_4/.27O_2/.60CO_2) blend at 985 K.

Another important validation test of the chemical kinetic mechanisms is in the production of CO which is expected to be significant at the near stoichiometric conditions of the Allam cycle. For this comparison, freely propagating laminar speed calculations as discussed earlier were performed for the same initial conditions as the ignition delay time calculations (300 bar, 985 K, *phi*=1, O_2=27%) and CO concentration was plotted as a function of spatial coordinate within the flame and shown in Figure 8. In the figure, the flame is propagating from right to left. All of the skeletal mechanism do a very good job of predicting the CO concentration profile relative to the parent mechanism, especially in the post flame zone where the temperature is roughly 2700 K. The calculation with GRI 3.0 showed slightly lower peak CO concentrations, but good agreement in the post flame zone.

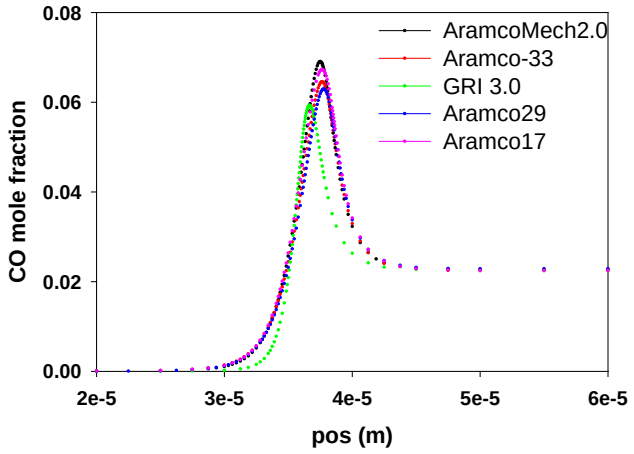

Figure 8: Calculated CO mole fraction profiles in a premixed laminar flame for several detailed and skeletal mechanisms. P=300 bar, T=985 K, .13CH_4/.27O_2/.60CO_2 mixture.

CFD LES Simulations

In order to better understand the nature of high pressure oxy combustion, a series of Large Eddy Simulations (LES) were conducted at Allam cycle conditions with various oxygen concentrations (Table 1). Large Eddy Simulation is generally regarded as a superior approach for modeling turbulent flows and allows for direct simulation of the larger turbulent length scales, which are more geometry dependent, while modeling the more homogeneous smaller scales. The transient nature of LES also allows for capturing unsteady phenomenon such as thermo-acoustic instabilities.

In all three cases described in Table 1, the total flowrates of methane, oxygen and carbon dioxide in the combustor were kept constant. The only difference was the flow split of CO_2 between the wall purge and the injectors. The methane flowrate was 1 kg/s corresponding to a nominal heat output of 50 MW and a mean combustor exit temperature of about 1520 K and global equivalence ratio of 0.95.

ANSYS Fluent 16.2 was again used with a LES turbulence modeling approach without any sub-grid combustion model. This assumes that mixing on the sub-grid level is fast compared to chemical reactions. The 17-species skeletal mechanism derived from Saudi Aramco 2.0 was used for the chemical kinetics. A bounded central differencing scheme was used for discretization of the momentum equation and second order upwinding was used for energy and species. A second order implicit backwards differencing scheme was used for the temporal discretization with a time step of 5 μsec and a dynamic kinetic energy transport model was used for the sub-grid viscosity. The code was run with the pressure based solver assuming compressible, ideal gas behavior. The assumption of ideal gas was deemed to be reasonable since the temperatures in the combustor are well above the critical point for any of the reactant species.

Figure 9 shows a series of snapshots of temperature for the three cases run with decreasing O_2 concentration in the injectors. These realizations are representative of the flow once it has reached a quasi-steady condition. Note that the mean combustor exit temperature (1520 K) was roughly the same for all three cases since the total flowrates of CH_4, O_2 and CO_2 was the same.

Figure 9 shows that at the highest O_2 concentration of 31% there appears to be a lifted flame in the combustor with peak flame temperatures just slightly above the adiabatic flame temperature for this mixture (2690 K). The sequence of snapshots shows the transition from a lifted turbulent flame at the highest O_2 volumetric concentration of 31% to more of an auto ignition type of process at the lowest oxygen concentration of 9%. Lowering the O_2 concentration causes a significant decrease in laminar flame speed to the point where a flame can no longer be sustained. Also, as more CO_2 is diverted from the wall purge to the injector flow, the injector exit velocity increases and tends to push the combustion zone further downstream. At the lowest O_2 concentration, the turbulent mixing is fast relative to the chemical reaction rates (low *Da* number) and auto ignition is achieved at some distance downstream from the injector faceplate once the ignition delay time has been surpassed (~ 2.5 msec). The flowfield for case 3 is somewhat more complex than the other two as the high velocity in the core of the flow creates a recirculation zone along the walls pulling hot combustion products back into the incoming flow.

The intermediate O_2 concentration (case 2) shows behavior somewhere between the high and low O_2 cases and it appears that the heat release is occurring with a combination of thickened turbulent flamelets and stirred reactor type of behavior.

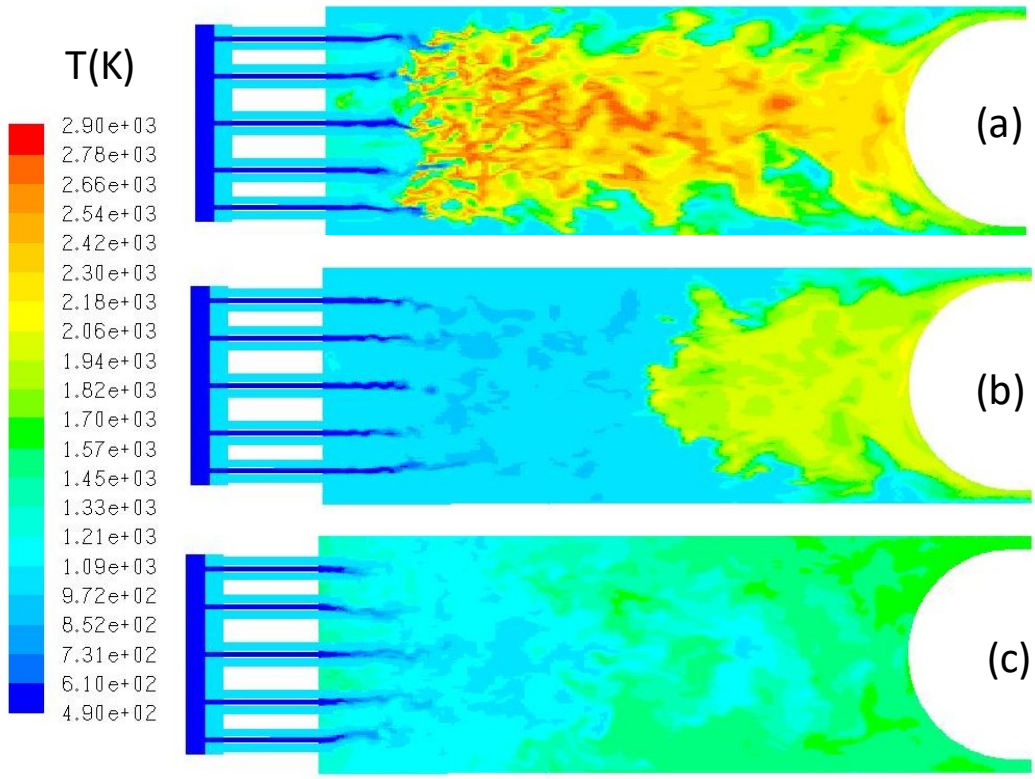

Figure 9: Instantaneous temperature contours through the center of the combustor for the three injector oxygen concentrations listed in Table 1. (a)=31%O_2, (b)=18%O_2 and (c)=9%O_2.

Instantaneous snapshots of CO mass fraction are shown in Figure 10. The change in O_2 concentration has a pronounced effect on CO production with peak CO concentration scaling with peak flame temperature. The peak CO concentration for the 31% O_2 case is very close to the calculated equilibrium concentration (Y_{CO2}=0.026) at the peak flame temperature and stoichiometric mixture ratio. The peak CO concentrations for cases 2 and 3 are somewhat higher than the calculated equilibrium values.

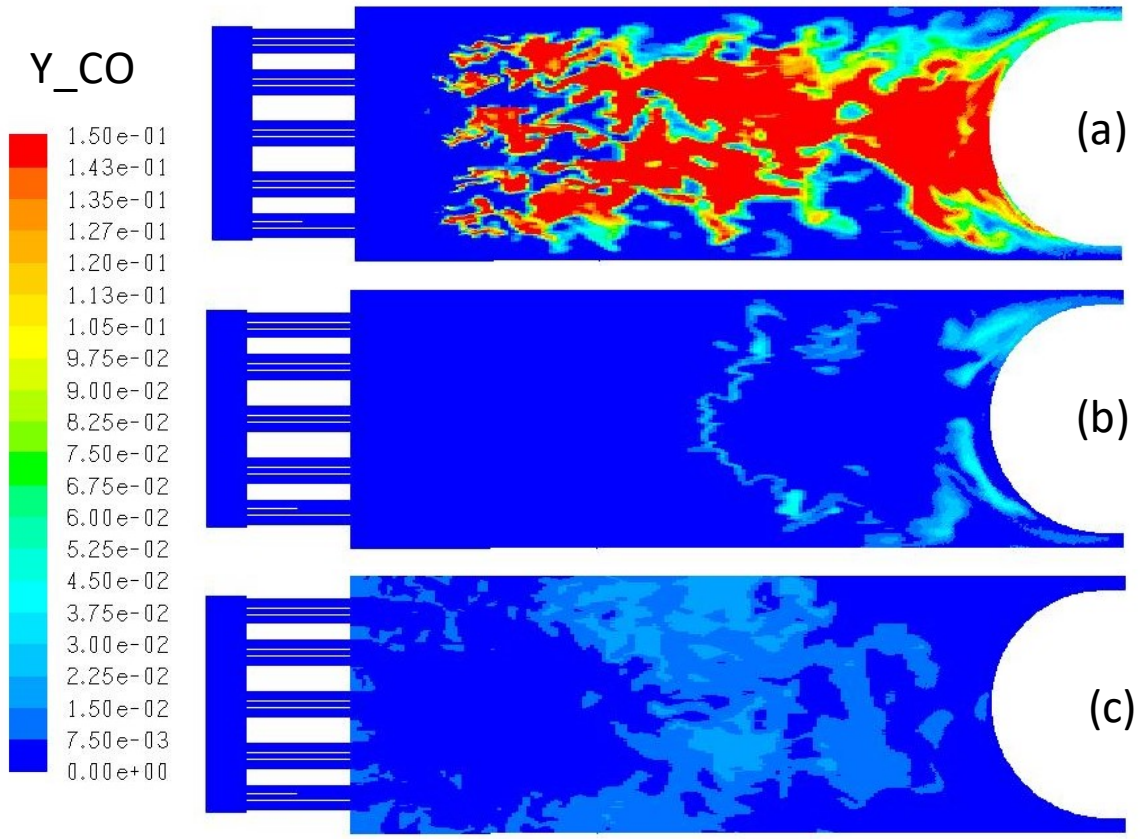

Figure 10: Instantaneous CO mass fraction contours through the center of the combustor for the three injector oxygen concentrations listed in Table 1. (a)=31%O_2, (b)=18%O_2 and (c)=9%O_2.

Conclusions

High-pressure oxy-combustion for direct-fired sCO_2 cycles presents some distinct challenges due to the very unique conditions and lack of experimental data available for validation. Pressure has been shown to drastically alter laminar flame properties by slowing and thinning the flame and increasing the extinction strain rate. Ignition delay time was found to decrease significantly with increasing pressure. While there are no detailed chemical kinetic mechanisms readily available that have been validated at very high pressure with CO_2 dilution, some mechanisms, such as the Saudi Aramco mechanism discussed here have

some validity at elevated pressure and have been used to develop skeletal mechanisms for use in CFD simulations.

An estimation of turbulent and chemical time and length scales has been carried out for a canonical combustor in an effort to characterize the range of combustion regimes anticipated to be found in an sCO_2 combustor. While these scales would be expected to vary considerably with combustor geometry and operating conditions, this approach at least provides a starting point in selecting appropriate combustion models for detailed CFD simulations. The analysis indicates that combustion may vary between the corrugated flame regime to the stirred reactor regime on the Borghi phase diagram. The range is the result of the possible variations of oxygen concentration in the combustion zone due to the fact that the oxygen from the air separation unit and the recycled CO_2 may be mixed in any proportion from nearly pure oxygen to an O_2 content as low as 7% by volume for the conditions of the Allam cycle. In practicality, the use of pure oxygen is unlikely due to the inherent dangers of oxygen fires at high pressures and temperature so an upper limit of 30% O_2 by volume may be more realistic.

Lastly, a series of LES simulations was carried out to examine the effect of oxygen concentration through the manipulation of the CO_2 flow split between the wall cooling purge and the injectors. Decreasing O_2 concentration and increasing injector velocity was found to shift the combustion regime from a turbulent flame, which would be governed by flame speed to a stirred reactor which would be more dependent on ignition delay time. Production of CO was also found to be strongly sensitive to O_2 concentration through changes in peak flame temperature.

References

1. "Trent 1000 Infographic", Rolls-Royce, http://www.rolls-royce.com/site-services/images/trent-1000-infographic.aspx.
2. "Main Propulsion System (MPS)", Shuttle Press Kit, Boeing, NASA & United Space Alliance, Oct. 6, 1998, www.shuttlepresskit.com/scom/216.pdf.
3. Allam, R. J., *et. al*., "High Efficiency and Low Cost of Electricity Generation From Fossil Fuels While Eliminating Atmospheric Emissions, Including Carbon Dioxide", Energy Pocedia, **37,** 2013, pp. 1135-1149.
4. Allam, R.J., Fetvedt, J.E., Forrest, B.A. and Freed, D.A., "The Oxy-Fuel, Supercritical CO2 Allam Cycle: New Cycle Developments to Produce Even Lower-Cost Electricity from Fossil Fules Without Atmospheric Emissions", Proceedings of ASME Turbo Expo 2014, GT2014-26952, June 16-20, Dusseldorf, Germany.
5. David G. Goodwin, Harry K. Moffat, and Raymond L. Speth. *Cantera: An object- oriented software toolkit for chemical kinetics, thermodynamics, and transport processes*. http://www.cantera.org, 2017. Version 2.3.0. doi:10.5281/zenodo.170284
6. Smith, G. P., Golden, D. M., Frenklach, M., Moriarty, N. W., Eiteneer, B., Goldenberg, M., Bowman, C. T., Hanson, R. K., Song, S., Gardiner Jr.,W. C., Lissianski, V., and Qin, Z., GRI-Mech homepage, Gas Research Institute, Chicago, 1999, www.me.berkeley.edu/gri_mech/.
7. W.K. Metcalfe, S.M. Burke, S.S. Ahmed, H.J. Curran, " A hierarchical and comparative kinetic modeling study of C_1–C_2 hydrocarbon and oxygenated fuels", Int. J. Chem. Kinet. (2013) 45(10) 638–675.

8. G. Rozenchan, D.I. Zhu, C.K. Law and S.D. Tse " Outward Propagation, Burning Velocities, and Chemical Effects of Methane Flames up to 60 atm", Proc. Comb. Inst., Vol 29, 2002, pp. 1461-1469.
9. E.L. Petersen, D.F. Davidson and R.K. Hanson, "Ignition Delay Times of Ram Accelerator CH4/O2/diluent Mixtures", J. Prop. Power, Vol. 15, No. 1, pp.82-91, 1999.
10. C. Sorusbay, "Spark Ignition Engine Combustion", MAK 652E Lecture, Istanbul Technical University,
11. Theoretical and Numerical Combustion, Poinsot and Veynante, 3rd edition, CERFACS, 2012.
12. ANSYS Fluent, Release 16.2.